

# **AUTO-DERIVATION OF IN-SHORE AND CHANNEL WATER DEPTH VIA AERIAL IMAGES: A LOW-COST APPROACH USING ARTIFICIAL NEURAL NETWORKS**

**Thi Nguyen<sup>1</sup>, Peter Wheeler<sup>1</sup>, Jim Peterson<sup>1</sup>, Lee Gordon-Brown<sup>2</sup>**

<sup>1</sup>Centre for GIS, School of Geography and Environmental Science,  
Monash University, Victoria, Australia

thi.nguyenthanh@gmail.com, pjwhe1@student.monash.edu.au,  
jim.peterson@arts.monash.edu.au

<sup>2</sup>Department of Econometrics and Business Statistics,  
Monash University, Victoria, Australia  
lee.gordon-brown@buseco.monash.edu.au

## **ABSTRACT**

Coastal zone isobathic pattern change monitoring provides coastal scientists, coastal engineers, and coastal managers with morphometric information of wide-ranging application. Even if the coastal management decision support team has access to such data, it may not have the temporal resolution, or the time series continuity to span the duration of cyclic trends of relevance in documenting and predicting rates and magnitudes of change. For some coastal zones, certain archival data sets, might yield such improvement to the derivable record, thereby extending its value. In these terms, we report here an approach of combining the data-integration power of Geographic Information System (GIS) with the “learning power” of Artificial Neural Networks (ANN) for bathymetry automation using vertical real-colour aerial images as input data. Calibration of spectral signatures for depth was achieved by identifying image pixels corresponding to spatial points of known water depth. The rules of mapping from colour to depth were established and held by deployment of an artificial neural network (ANN) training process. It is shown that by applying these rules, pixel by pixel, for any new images covering the same spatial area, the depth pattern at the image snap-shot time can be derived. This approach was tested with spatial data representing the Lakes Entrance sector of the coast of Victoria, Australia. Results demonstrated the potential of this machine-learning technique, i.e. artificial neural networks, for dealing with estimation problems, especially regarding those calling on data assembled via deployment of spatial and/or geographic science. It is a low-cost procedure offering potential to give significant advantage not only in time-series archive assembly but also for bathymetric survey that does not require the accuracy (and expense) that can now be obtained by application of (GPS-controlled) detailed sounding methods.

## **INTRODUCTION**

Hydrography is the science that deals with all measurements and descriptions of the physical features of bodies of water and their littoral. Marine or hydrographic surveys support a variety of activities such as port and harbor maintenance (dredging), coastal

engineering (beach erosion and replenishment studies), coastal zone management, and offshore resource development. However, typical hydrographic surveys carried out for the purpose of navigation differ from other surveys in terms of techniques used, and in the nature of the final desired output. For example, bathymetric surveys are aimed, primarily, at collecting depth data. The earliest charts depicting underwater topography were assembled from sounding with a lead-line. Later, continuous trace electronic sounding devices were used. The latest depth-sounding technology yields a geocoded point-cloud file that can be taken directly into GIS.

The bathymetric survey archive is very useful for monitoring changes in sediment distribution and channel navigability. The more surveys in the archive, the closer it comes to representing the range of changes that have occurred, and the better the archive can support efforts to arrive at explanatory predictions. In that spatial data referring to coastal areas includes not only bathymetric charts, but also air photos, some interest attaches to exploiting any apparent scope for deriving isobathic data from imagery.

This study combines GIS (Lo & Yeung, 2007) and an artificial intelligence technique, machine learning via deployment of Artificial Neural Networks (ANNs) (Freeman & Skapura, 1991; Madan *et al.*, 2003), to extract depth data from archival imagery. An ANN is an information processing paradigm that is inspired by the way biological nervous systems, such as the brain, process information. The key element of this paradigm is the novel structure of its information processing system. It is composed of a large number of highly interconnected processing elements (neurons) working in unison to solve specific problems. ANNs, like people, learn by example. An ANN is configured for a specific application, such as pattern recognition or data classification, through a learning process. Learning in biological systems involves adjustments to the synaptic connections that exist among the neurons. This is also true of ANNs. The learning capability of an ANN will be harnessed in this research to derive, from (coloured) air photo, pixel by pixel, a cloud-point of water-depth values.

## **ARTIFICIAL NEURAL NETWORKS FOR AUTOMATING WATER DEPTH PATTERNS FROM PIXEL SPECTRAL SIGNATURES**

### **ANN Configuration**

Neural network architecture of has been applied to a broad range of practical problems. This study focuses on the Recurrent Fuzzy Neural Network (RFNN) (Mandic & Chambers, 2001; Medsker & Jain, 2001) approach. It has become a powerful tool for solving real-world problems in the area of forecasting, identification, control, image recognition and other problem solving associated with high levels of uncertainty (Xiaolin & Balasubramaniam, 2008). This is related to the fact that the RFNN paradigm combines the capability of fuzzy reasoning in handling uncertain information and the capability of pure neural networks to learn from experiments. The RFNN approach may allow for deployment of smaller (faster) networks, and thereby faster convergence as compared to results from deployment of the ordinary neural network approach.

The RFNN model, depicted in Figure 1, is structured for approximating the nonlinear function  $F: R^N \rightarrow R^P$  where  $N$  and  $P$  are the number of inputs and outputs,

respectively. There are four layers of RFNNs in total; each layer consists of one or more nodes, i.e. neurons that are computational units.

Denote  $u_i^{(k)}$  and  $o_i^{(k)}$  as input and output values of the  $i^{th}$  node in the  $k^{th}$  layer.

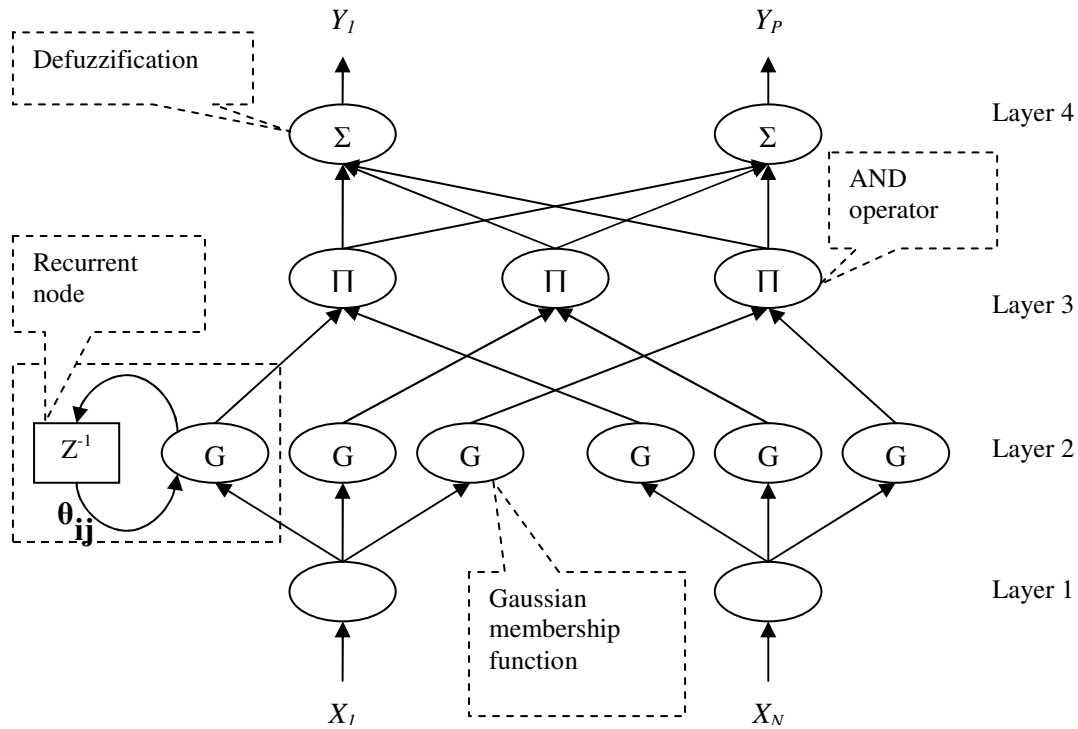


Fig. 1: The four layers in the RFNN configuration. Each node in layer 2 at time point ( $t$ ) contains its previous state at time point ( $t - 1$ ) and is termed a “recurrent” node.

**Layer 1**

$$o_i^{(1)} = u_i^{(1)} = x_i(t), i = 1 \div N$$

**Layer 2**

$$o_{ij}^{(2)} = \exp\left[-\frac{(u_{ij}^{(2)} - m_{ij})^2}{(\sigma_{ij})^2}\right], i = 1 \div N, j = 1 \div M$$

where  $M$  is the number of fuzzy rules,  $m_{ij}$  and  $\sigma_{ij}$  are the centre and width of the Gaussian membership function, and

$$u_{ij}^{(2)}(t) = o_i^{(1)} + \theta_{ij} o_{ij}^{(2)}(t-1)$$

with  $\theta_{ij}$  is the weight of the recurrent node.

$$o_{ij}^{(2)} = \exp\left[-\frac{[x_i(t) + \theta_{ij} o_{ij}^{(2)}(t-1) - m_{ij}]^2}{(\sigma_{ij})^2}\right], i = 1 \div N, j = 1 \div M$$

**Layer 3**

The operator AND is used to multiply outputs of layer 2 together.

$$o_j^{(3)} = \prod_{i=1}^N o_{ij}^{(2)} = \prod_{i=1}^N \exp \left[ -\frac{[x_i(t) + \theta_{ij} o_{ij}^2(t-1) - m_{ij}]^2}{(\sigma_{ij})^2} \right], i = 1 \div N, j = 1 \div M$$

#### Layer 4

The nodes on layer 4 undertake the defuzzification function

$$y_k = o_k^{(4)} = \sum_{j=1}^M u_{jk}^{(4)} w_{jk} = \sum_{j=1}^M o_j^{(3)} w_{jk} = \sum_{j=1}^M w_{jk} \prod_{i=1}^N \exp \left[ -\frac{[x_i(t) + \theta_{ij} o_{ij}^2(t-1) - m_{ij}]^2}{(\sigma_{ij})^2} \right]$$

All four types of parameters  $m_{ij}$ ,  $\sigma_{ij}$ ,  $\theta_{ij}$  and  $w_{jk}$  need to be trained over the whole  $(N + N.M + M + P)$  set of nodes of the RFNN.

### RFNN Training Process

Relying upon the aim of minimizing the squared error function, the supervised gradient descent learning approach was utilized to tune the parameters:

$$E(x) = \frac{1}{2} (f(x) - F(x))^2 = \frac{1}{2} \left( \text{observed} - \text{estimated}^{(4)} \right)^2$$

where  $f(x) = \text{observed}$  is the observed (real) value and  $F(x) = \text{estimated}^{(4)}$  is the value computed from the RFNN and is output at the fourth layer.

The parameters are updated via the formula:

$$\xi(t+1) = \xi(t) - \mu_t \frac{\partial E}{\partial \xi}$$

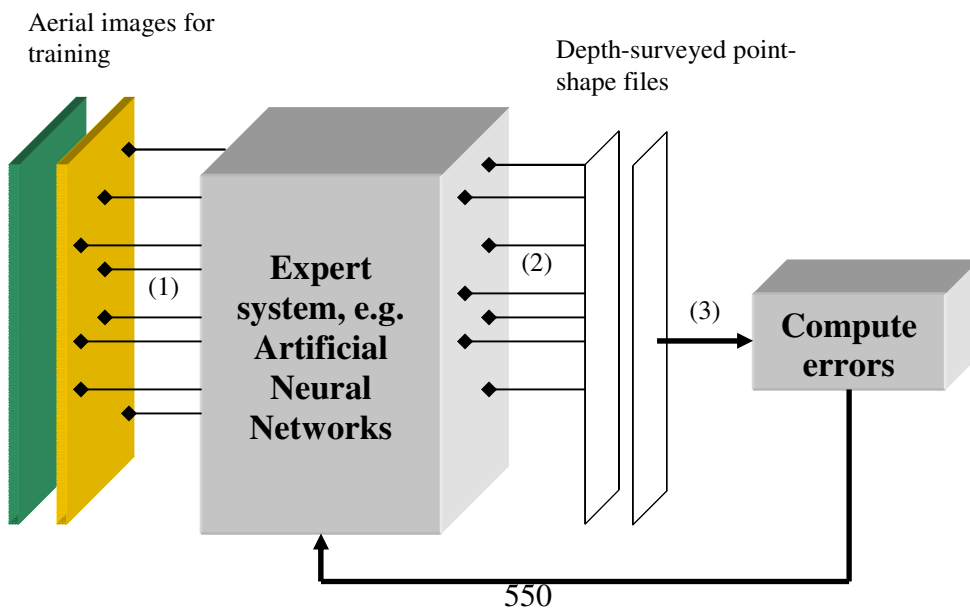
with  $\mu_t$  as learning rate at iteration  $t$ .

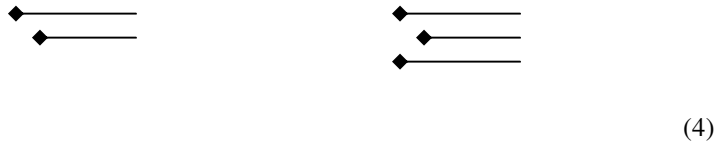
The momentum technique (Qian, 1999) was also integrated in the parameters tuning process to increase the speed of convergence. The learning formula with momentum is as follows:

$$\xi(t+1) = \xi(t) - \mu_t \frac{\partial E}{\partial \xi} + \varepsilon \cdot \Delta \xi(t)$$

where  $\varepsilon$  is the momentum coefficient.

### Application to Auto-Derivation of Water Depth





Modify the model

Fig. 2: Training process of the RFNN to simulate mapping rules for derivation of depth values from colour values (RGB spectral signatures) (see Figure 3).

The process whereby the RFNN training yields knowledge useful for auto-derivation (image pixel by pixel) of depth is illustrated in Figure 2.

The first step is to read the pixel data at image points for which coeval depths have been surveyed.

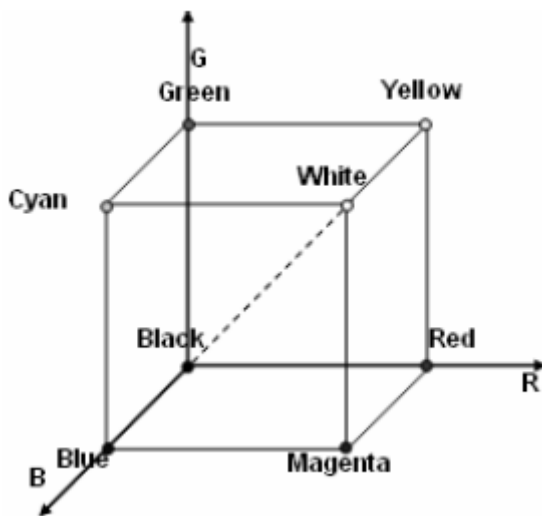
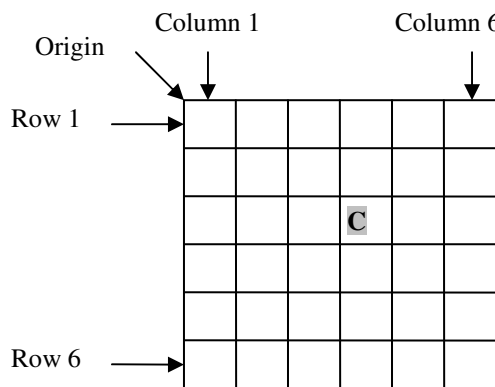


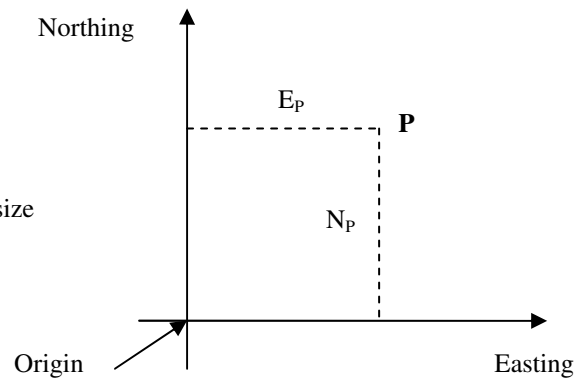
Fig. 3: Technical aspect of the RGB colour model

The procedure for identification of the image pixels for which calibration depths are available is shown in Figure 4. The data from pixel reading are parsed into three colour-band values: red, green and blue. The next step is to input these three primary colours of pixels into the model for estimation of depth value. The third step is to compare the estimated depth with real (surveyed) depth. From the obtained error, the learning algorithm described above is applied to train the model. That is the main task of the fourth step. Reiteration eventually brings convergence. An expert system with the ability of depth estimation for any new images emerges after completion of this training step.



Position of C = (row, column) = (3, 4)

(a) A raster coordinate system



Position of P = (E<sub>p</sub>, N<sub>p</sub>)

(b) A map coordinate system

Fig. 4: The raster and map coordinate systems

## EXPERIMENTS AND RESULTS

Three high quality “snapshots” (September 2006, June 2007, and September 2007) of colour orthophoto mosaics (pixel resolution 0.4m) are matched with coeval point-shape files data. Figures 5-8 show the collected data in June 2007 and GIS techniques for how to extract necessary data from the raw data.

For the sake of comparison, two training and testing scenarios have been investigated: for the first, the training and testing images are the same whereas for the second scenario, the applicability of training derived from one image was tested on a different image from the same shore zone. Training and testing sample site selection is based on the quality of image pixels that overlap surveyed depth points in the corresponding (bathymetric) shape files. The statistics, in terms of both experimental data and errors, are assembled case-by-case (Table 1 and 2). The lower the error reported, the higher the accuracy of derived depth. Following, are formula for the mean absolute error (MAE) considered here as the evaluation criterion.

$$MAE = \frac{1}{n} \sum_{i=1}^n |estimated_i - surveyed_i|$$

where  $n$  is the number of testing samples,  $estimated_i$  and  $surveyed_i$  are the estimated and surveyed depths, respectively.

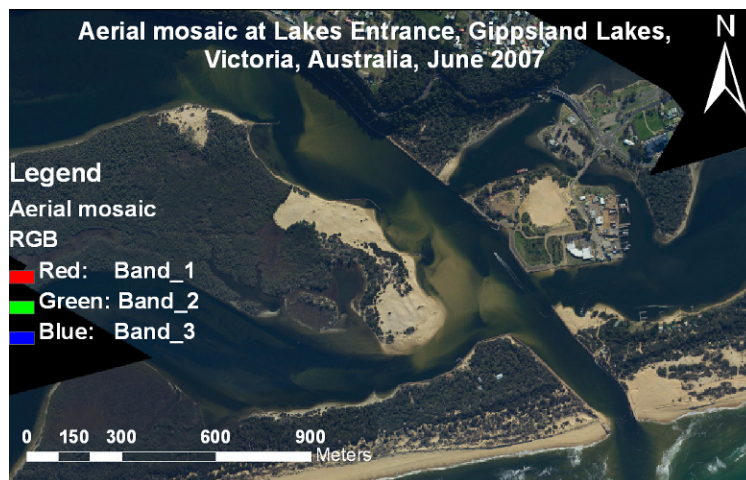


Fig. 5: Aerial mosaic in June 2007 showing the Lakes Entrance harbour entrance. Some colour noise in images will be rejected before inputting to the RFNN.

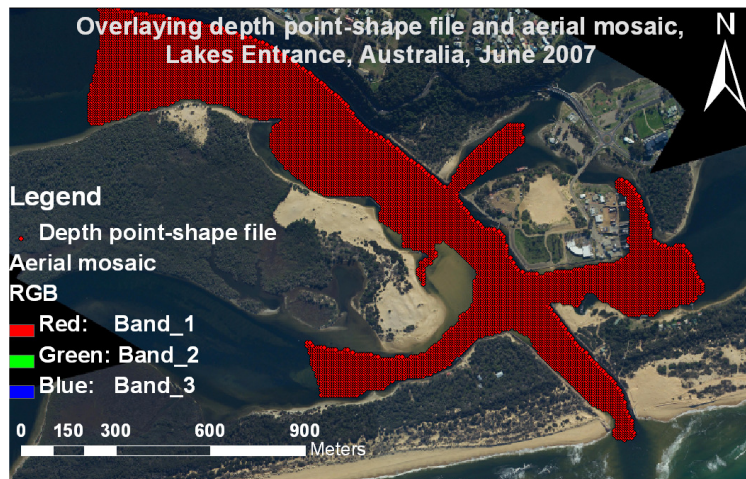


Fig. 6: Depth point-shape file projected in GDA\_1994\_MGA\_Zone\_55 is overlaid on the aerial mosaic that is captured at the same time as the depth point cloud.

Attributes of Depth shape file						
FID	Shape	PointNumbe	Elevation	Locationx	Locationy	
0	Point ZM	5234	-1.752	585585	5805840	
1	Point ZM	5235	-1.393	585562.5	5805847.5	
2	Point ZM	5236	-1.58	585570	5805847.5	
3	Point ZM	5237	-1.983	585577.5	5805847.5	
4	Point ZM	5238	-2.305	585585	5805847.5	
5	Point ZM	5239	-2.136	585592.5	5805847.5	
6	Point ZM	5240	-2.477	585600	5805847.5	
7	Point ZM	5241	-2.668	585607.5	5805847.5	
8	Point ZM	5242	-1.218	585555	5805855	
9	Point ZM	5243	-1.577	585562.5	5805855	
10	Point ZM	5244	-1.937	585570	5805855	
11	Point ZM	5245	-2.254	585577.5	5805855	
12	Point ZM	8061	-2.506	585585	5805855	

Fig. 7: Attributes of depth point-shape file. The location ( $x, y$ ) (real spatial coordinates) of each point is transformed to indicate exactly position of corresponding pixel on the image based on the defined projection: GDA\_1994\_MGA\_Zone\_55. Water depths at 10450 points have been surveyed beforehand. The number of points selected for the training process however is limited based on the sampling criteria.

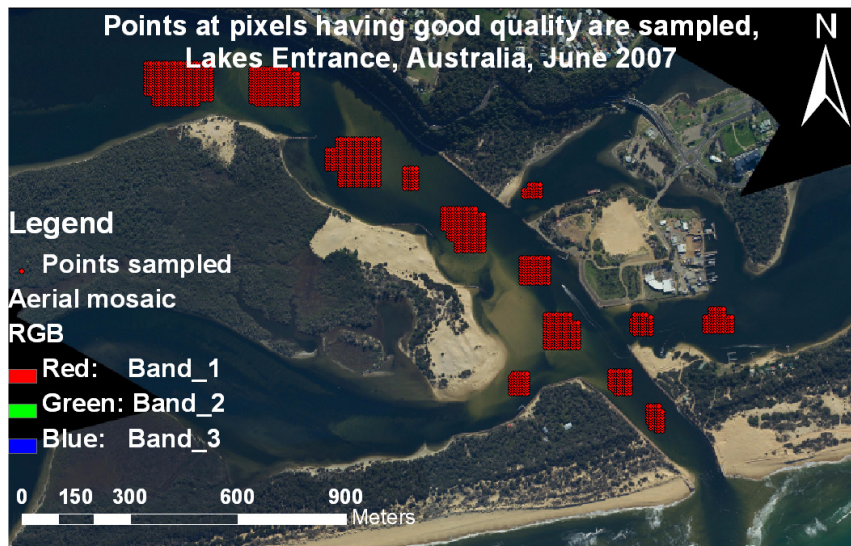


Fig. 8: An example of sampling process in the June 2007 ‘snapshot’. Points are sampled relying on the quality of the image pixels and ensuring that a broad range of depth (or colour) is taken into account.

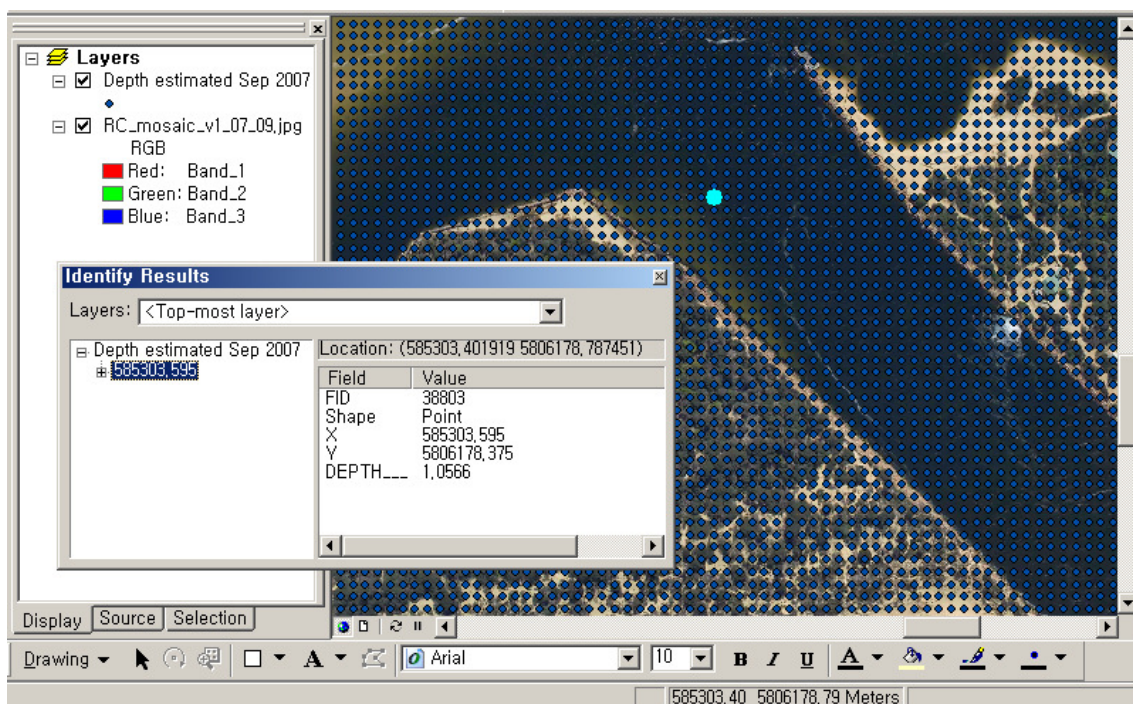


Fig. 9: Depths estimated based on aerial mosaic in September 2007. The depth point-shape file is created with spatial interval at 2.2 meters for both x and y dimensions. The denser and/or sparser point-shape files also can be made depending absolutely on the aim of the depth-deriving exercise. Points positioned over good-quality image pixels (without noise) are selected for testing statistics.

Tab. 1: Experimental data and testing results for scenario 1: training and testing images are the same

Scenario 1	Test 1		Test 2	
	Aerial mosaic	Sample number	Aerial mosaic	Sample number
Training	September 2006	400	June 2007	400
Testing	September 2006	1400	June 2007	1500
Error	0.357 m		0.345 m	

Tab. 2: Experimental data and testing results for scenario 2: training and testing images are different from each other

Scenario 2	Test 3		Test 4	
	Aerial mosaic	Sample number	Aerial mosaic	Sample number
Training	September 2006	500	September 2006	500
			June 2007	500
Testing	June 2007	1400	September 2007	1500
Error	0.724 m		0.903 m	

In scenario 1, two tests were performed using September 2006 and June 2007 mosaics. The MAE obtained are nearly the same, approximately 0.35 meters, for both tests. With regard to scenario 2, where training and testing images are different, the error obtained is higher than for the tests in scenario 1. Test 3 uses the September 2006 mosaic for training and the June 2007 mosaic for testing. An error of around 0.72 meters emerged. In case of test 4, two snapshots are included for training (September 2006 and June 2007) and the September 2007 image reserved for testing. The MAE in this case is about 0.9 meters, which is higher than the error in previous tests. The inevitable discrepancy between images of snapshots would account for the difference because depth changes will have taken place between June and September (Wheeler *et al.*, 2009). In addition, it is important to note that, in the same test, the error and thus the accuracy are possibly different depending on the nature of the sampling dataset. A “good” input dataset can lead to a better result than reported herein. In contrast, some other dataset may lead to less accurate results. This shows that the accuracy of the proposed approach is highly sensitive to the quality of input data. Clearly, this approach must be reserved for waterways for which regular calibration is available and for which many days are available for air photography to record images of waterways that are free of suspended sediment. This approach would not be very useful for surf-zone monitoring, unless the calibration referred to density of suspended sediment.

## CONCLUSIONS

Based on the colour values of pixels (three colour bands) and the real (surveyed) depth of the corresponding position over the waters, the ANN system as deployed for this experiment, acquired the knowledge needed for producing consistent depth estimation: mapping from image colour to water depth. The accuracy of the system is seen to

depend not only on its structure but also on the nature and quality of the input data. In this case, much depends on the quality of aerial images used. Take, for example, the water colouring at the time of data capture. As the water is too dark, the sea/inlet floor cannot be seen and hence the output is unreliable. The extent to which the calibration of isobathic data is less than synchronous with the image data snap-shot, is the extent to which error can certainly be expected. The calibration images thus should be captured at the same time as the depth soundings ideally. Once tested for application between calibration episodes, water depth monitoring may be served by taking the approach exemplified here.

In practice, most hydrographic surveys are conducted based on the guidance of the International Hydrographic Organization (IHO) accuracy standards for hydro-data. According to the latest version (No. 44) of these standards, the allowable error for depth measurements is 0.3 meters for 0 to 30 meters depth, and 1% of depth deeper than 30 meters. Lakes Entrance channels, the water depths are < 30 meters, and so the results of the experiments were not satisfactory in terms of IHO standards. Nevertheless, as a low-cost depth auto-derivation, the accuracy achieved is acceptable for trend monitoring when port authorities do not have regular soundings taken. Costs can be minimized by selective depth sounding (Z) with ground control (X/Y) at the same time as aerial photos are captured, as they would be from time to time for purposes separate from those of port maintenance. Large shallow water (littoral) areas can be modeled for low cost using this method. On the contrary, it is expensive to hire hydrographic sounding equipment and also have aerial photos flown.

Potentially, the discrepancy between the quality of images as input to this approach refers largely to the difference between the turbidity of water depicted in the 'snapshots'. Because many air photo archives are now distributed and data acquisition is mostly on a just-in-time basis and in reference to very specific areas, and catchment and coastal stakeholder collaborations, there are both incentive and opportunity for port authorities to ask that image acquisition to be scheduled for times of slack tide.

## REFERENCES

- Freeman, J.A. and Skapura, D.M., 1991. *Neural Networks: Algorithms, Applications, and Programming Techniques*. Addison-Wesley Publishing Company, Inc., USA.
- International Hydrographic Organization, 1998. *IHO Standards for Hydrographic Surveys*, Special Publication No. 44, 4th Edition.
- Lo, C.P. and Yeung, A.K.W., 2007. *Concepts and Techniques of Geographic Information Systems*. Second Edition, Pearson Prentice Hall.
- Madan, M.G., Liang, J. and Noriyasu, H., 2003. *Static and Dynamic Neural Networks*. John Wiley and Sons, Inc., New York, USA.
- Mandic, D.P. and Chambers, J.A., 2001. *Recurrent Neural Networks for Prediction*. John Wiley & Sons, Ltd., West Sussex, England.
- Medsker, L.R. and Jain, L.C. 2001. *Recurrent Neural Networks: Design and Applications*. CRC Press LLC, Florida, USA.

- Qian, N., 1999. "On the momentum term in gradient descent learning algorithms", *Neural networks*, vol. 12, pp. 145-151.
- Wheeler, P.J., Peterson, J.A. and Gordon-Brown, L.N., (2009 submitted). "Flood-tide delta morphological change at the Gippsland Lakes artificial entrance, Australia (1889-2009)", *Australian Geographer*.
- Xiaolin Hu and P. Balasubramaniam, 2008. *Recurrent Neural Networks*, ISBN 978-953-7619-08-4, 400 pages, I-Tech, Vienna, Austria.

## **BRIEF BIOGRAPHY OF PRESENTER**

Thi Nguyen, B.Eng. (Computer Science and Engineering) studied at the University of Technology, Vietnam National University Ho Chi Minh City between 2002 and 2007. Following graduation, he was appointed lecturer of the Department of Applied Geomatics, Nong Lam University, Vietnam. For three months (2007-08) he was a visiting academic at the Centre for GIS, School of Geography and Environmental Science, Monash University, Australia. His research expertise includes devising and testing applications of spatial technologies for mapping and modeling changing environments with special reference to the coastal zone. Currently, this interest is converging with his other interests: applications of soft computing techniques to GIS and Remote Sensing and, as we see from the paper he is about to present, joint applications of fuzzy maths and neural networks.